G-protein modulation of N-type calcium channel gating current in human embryonic kidney cells (HEK 293)

Lisa P. Jones, Parag G. Patil, Terry P. Snutch* and David T. Yue†

*Program in Molecular and Cellular Systems Physiology, Department of Biomedical Engineering, Johns Hopkins University School of Medicine, 720 Rutland Avenue, Baltimore, MD 21205, USA and *University of British Columbia, Vancouver, British Columbia V6T 173, Canada*

1. Voltage-dependent inhibition of N-type calcium currents by G-proteins contributes importantly to presynaptic inhibition. To examine the effect of G-proteins on key intermediary transitions leading to channel opening, we measured both gating and ionic currents arising from recombinant N-type channels (α_{1B}, β_{1b} and α_2) expressed in transiently transfected human embryonic kidney cells (HEK 293). Recombinant expression of a homogeneous population of channels provided a favourable system for rigorous examination of the mechanisms underlying G-protein modulation.

2. During intracellular dialysis with GTPγS to activate G-proteins, ionic currents demonstrated classic features of voltage-dependent inhibition, i.e. strong depolarizing prepulses increased ionic currents and produced hyperpolarizing shifts in the voltage-dependent activation of ionic current. No such effects were observed with GDPβS present to minimize G-protein activity.

3. Gating currents were clearly resolved after ionic current blockade with 0·1 mM free La^{3+}, enabling this first report of gating charge translocation arising exclusively from N-type channels. G-proteins decreased the amplitude of gating currents and produced depolarizing shifts in the voltage-dependent activation of gating charge movement. However, the greatest effect was to induce a ~20 mV separation between the voltage-dependent activation of gating charge movement and ionic current. Strong depolarizing prepulses largely reversed these effects. These modulatory features provide telling clues about the kinetic steps affected by G-proteins because gating currents arise from the movement of voltage sensors that trigger channel activation.

4. The mechanistic implications of concomitant G-protein-mediated changes in gating and ionic currents are discussed. We argue that G-proteins act to inhibit both voltage-sensor movement and the transduction of voltage-sensor activation into channel opening.

The voltage-dependent inhibition of N-type calcium channels by G-proteins contributes importantly to modulation of neurotransmitter release, and thereby synaptic strength (Hille, 1994). Although it has been established that this modulation involves G-protein $\beta\gamma$-subunits (Ikeda, 1996; Herlitze, Garcia, Mackie, Hille, Scheuer & Catterall, 1996) acting by a fast, membrane-delimited pathway (Lipscombe, Kongsamut & Tsien, 1989), key features of the effects of G-proteins on channel operation remain unclear. Studies of N-type channel function have only examined ionic current flowing through channels, thus confining observations to the entry of channels into the open state(s). Such measurements permit only limited inferences about transitions among all the gating conformations that precede channel opening, especially those associated with the movement of voltage sensors that underlie channel activation. Resolution of gating current arising from voltage-sensor motion (Armstrong & Bezanilla, 1974) could provide direct information about how G-proteins affect the critical intermediary transitions that lead to channel opening. However, the coexistence of multiple species of voltage-gated channels in neurons has so far precluded isolation of N-type gating current. Here, we express recombinant N-type channels in mammalian HEK 293 cells to permit the first measurement of pure N-type channel gating current, both in the presence and absence of G-protein inhibition. We find that G-proteins act to retard not only voltage-sensor activation, but the transduction of voltage-sensor movement to channel opening.

† To whom correspondence should be addressed.

METHODS

Expression of N-type channels

HEK 293 cells, obtained from Dr Jeremy Nathans (Gorman, Gies & McCray, 1990), were grown at 37 °C in Dulbecco's modified Eagle's medium (Gibco), 10% fetal calf serum (Gibco), 1% L-glutamine (Sigma), 1% penicillin–streptomycin solution (P0906, Sigma), in 5% CO_2. Low passage number cells were used (< P20). cDNAs encoding channel subunits α_{1B} (rbB-II: Dubel *et al.* 1992), β_{1b} (Pragnell, Sakamoto, Jay & Campbell, 1991), and α_2 (Tomlinson, Stea, Bourinet, Charnet, Nargeot & Snutch, 1993) were subcloned into either a CMV-promotor expression plasmid (pGW1, British Biotechnologies, Cowley, Oxford, UK; for α_{1B} and β_{1b}), or a constitutively active metallothionine promoter expression plasmid (pZEM229R, Zymogenetics, Seattle, WA, USA; for α_2). HEK 293 cells were transiently transfected using a calcium phosphate precipitation procedure (Dhallan, Yau, Schrader & Reed, 1990) with 3, 1, and 12 μg of each plasmid, respectively, per 10 cm plate. More than 20% of transfected cells exhibited detectable high-threshold calcium currents.

There are two lines of strong evidence that all three calcium channel subunits were expressed. First, there is an extensive literature in which multiple cDNA constructs have been simultaneously expressed in HEK 293 cells, using a calcium-phosphate precipitation procedure. These include combinations of the GABA receptor subunits (Verdoorn, Draguhn, Ymer, Seeburg & Sakmann, 1990), subunits of the cyclic nucleotide-gated channels (Chen, Peng, Dhallan, Ahmed, Reed & Yau, 1993), as well as NMDA channels and a green fluorescent protein reporter gene (Marshall, Molloy, Moss, Howe & Hughes, 1995). In all these results, it appeared that a cell either expressed all cDNA products, or none. This result held true despite the fact that an appreciable fraction of cells failed to express any recombinant ion channel activity. Second, we found that transfection of α_{1B} alone failed to express any recombinant ion channel activity. Recombinant calcium current only arose when the β_{1b}-subunit was cotransfected. Hence, the β_{1b}-subunit must have been expressed in all cells yielding recombinant calcium current. Additional cotransfection of the α_2-subunit typically yielded severalfold larger currents, in agreement with results of Brust *et al.* (1993). Taken together, these two lines of evidence argue that all three calcium channel subunits were successfully coexpressed in our study.

'Mock-transfected' cells (in Fig. 2) were transfected with 30 μg of pBluescript (Stratagene, La Jolla, CA, USA). In our usual ionic current recording conditions (detailed below) we observed no high-threshold, voltage-gated calcium channel currents, even after cotransfection with β_{1b}- and α_2-subunits ($n = 32$ cells, over two independent rounds of transfection), or with the β_2-subunit alone ($n > 40$ cells; Patil, de Leon, Reed, Dubel, Snutch & Yue, 1996). In mock-transfected cells, we occasionally (~10% of cells) observed endogenous, low-threshold calcium channel currents of small amplitude (peak ionic current ~20 pA), as reported previously by Sun *et al.* (1994). Although endogenous currents of such small amplitude would contribute negligibly to our results, cells with low-threshold activity were nevertheless rejected. Although much higher levels of endogenous, low-threshold calcium current have been reported in HEK 293 cells by Berjukow, Doring, Froschmayr, Grabner, Glossmann & Hering (1996), their study used a different clone of HEK 293 cells (American Type Culture Collection, Rockville, MD, USA) with high passage number (> P32).

Electrophysiology

Whole-cell recordings were obtained at room temperature (20–22 °C) 48–72 h after transfection using patch-clamp techniques. The external solution contained (mM): 145 *N*-methyl-D-glucamine (NMG) aspartate, 10 glucose, 10 Hepes, 10 4-aminopyridine, 0·1 EGTA, pH adjusted to 7·4 with NMG. Either 2 mM $BaCl_2$ or 0·2 mM $LaCl_3$ and 2 mM $MgCl_2$ were added for ionic or gating current measurements, respectively. For experiments using ω-conotoxin GVIA (ω-CgTX, Alamone Labs, Jerusalem), 0·05% (w/v) fatty acid-free bovine serum albumin was added to the external solution. The bath solution was earthed by a 0·5 M KCl agar bridge attached to a Ag–AgCl wire. The internal solution contained (mM): 135 NMG-methanesulphonate ($MeSO_3$), 1 $MgCl_2$, 4 MgATP, 10 Hepes, 10 EGTA, pH adjusted to 7·3 with NMG. Either 300 μM GTPγS or 2 mM GDPβS was added to the internal solution. Measurements were started after > 10 min of dialysis with the internal solution. Series resistance was typically < 5 MΩ, and compensated 60–80%. Leak and capacity currents were subtracted by a $P/8$ protocol (ionic currents) or $P/-5$ protocol (gating currents). Voltage pulses were delivered every 10–15 s from a holding potential of −100 mV. Data were typically filtered at 10 kHz (−3 dB, 4-pole Bessel) and sampled at 50 kHz. Traces are displayed at a 5 kHz bandwidth, using further digital Gaussian filtering as required. In all cases, the junction potential between external and internal solutions was ~5 mV (Neher, 1992). To determine the true applied potential, this value should be added to the voltages in the figures and text.

For ionic currents, 2 mM $BaCl_2$ was the charge carrier throughout. Test depolarizations ranged from −70 to +70 mV, as illustrated for three test depolarizations within this range in the voltage protocol at the top of Fig. 1*A*. On alternate voltage commands, there was a 45 ms prepulse to +100 mV before the test pulse. The prepulse and the test pulse were separated by a 20 ms interpulse at −100 mV. Test pulses lasted 30 ms unless indicated otherwise. For each cell, plots of peak tail current at −50 mV (I_{tail}) *versus* test pulse voltage (V_{test}) were normalized by an estimate of maximal peak tail current (I_{max}). I_{max} was taken as the +50 mV value of dual-Boltzmann fits (see below) to I_{tail}–V_{test} data obtained with prepulse, rather than to the individual data point at +50 mV. Note that the same I_{max} was used to normalize all data (with or without prepulse) from a given cell. The resulting normalized relations are equivalent to relative conductance (G/G_{max}, where G and G_{max} are conductance and maximum conductance, respectively) expressed as a function of voltage (G–V curves). Such G–V curves were then averaged across cells. G–V plots are shifted to the right by +12 mV to account for the surface potential difference between solutions used to measure ionic and gating currents (detailed below). Ionic current records are shown without this shift.

For gating currents, ionic currents were blocked by the external solution containing 0·2 mM $LaCl_3$ (Bean & Riòs, 1989). The effective free La^{3+} concentration was 0·1 mM due to the presence of 0·1 mM EGTA in all external solutions. The voltage protocol was the same as for ionic currents, except that the test pulse duration was decreased to 20 ms, and repolarization was to −100 mV (Fig. 2*A*, top). Total charge moved during test depolarization (Q_{on}) was obtained by integrating over the entire depolarizing epoch, taking as the zero baseline the average current over the last 4–5 ms of the test pulse. Total charge moved during repolarization (Q_{off}) was calculated similarly. For each cell Q_{on}–V and Q_{off}–V curves were normalized by an estimate of maximal mobile charge (Q_{max}). Q_{max} was taken as the +50 mV value of the dual-Boltzmann fit (detailed below) to the Q_{off}–V data with prepulse. The same Q_{max} was used to normalize all data (± prepulse, Q_{on} and Q_{off}) from a given cell. Such normalized Q–V curves were averaged across cells.

To determine the difference in surface potential during ionic *versus* gating current measurements, ionic current was blocked by 2 μM ω-CgTX throughout. Q–V curves were then determined, first with

the external solution containing 2 mM $BaCl_2$ (e.g. Fig. 1*B*, inset), then with the external solution containing 0·2 mM $LaCl_3$ and 2 mM $MgCl_2$. The *Q–V* curve with 2 mM $BaCl_2$ was shifted to the left, but had an identical shape to the *Q–V* curve with 0·2 mM $LaCl_3$ and 2 mM $MgCl_2$. Moreover, the kinetics of gating currents were identical in the two solutions after accounting for the voltage shift, arguing that La^{3+} produced no intrinsic distortion of gating properties. Hence, the voltage shift required to fit the same dual-Boltzmann equation to both sets of data (12 ± 3 mV; $n = 3$ cells) was taken as a simple surface potential difference (not shown). For all gating current experiments used to assess the effects of G-proteins, we favoured the use of La^{3+} to ablate ionic current because its block was reversible whereas ω-CgTX block was not. We could thus recover ionic currents after gating current determinations, enabling checks for the stability of G-protein modulation.

Dual Boltzmann fits to either *G–V* or *Q–V* relations were performed with functions of the form:

$$f_{lo}(1 + \exp((Z_{lo}F/RT)(V_{½,lo} - V_{test})))^{-1} + f_{hi}(1 + \exp((Z_{hi}F/RT)(V_{½,hi} - V_{test})))^{-1},$$

where, for low- and high-threshold components, respectively, $V_{½,lo}$ and $V_{½,hi}$ are midpoints of activation, Z_{lo} and Z_{hi} are the effective valences, f_{lo} and f_{hi} are fractional amplitudes, and F, R and T have their usual meaning. Q_{on}–V data above +40 mV were sometimes unreliable and were therefore excluded. Fits were obtained using non-linear, least-squares minimization. All reported values are means ± S.E.M.

RESULTS

Modulation of ionic current by G-proteins

We have recently demonstrated that recombinant N-type channels (α_{1B}, β_{1b} and α_2) expressed in human embryonic kidney cells (HEK 293) can be inhibited by G-proteins in a voltage-dependent manner (Patil *et al.* 1996). Figure 1 illustrates the characteristic effects of G-proteins on recombinant N-type channel current in HEK 293 cells, with 2 mM $BaCl_2$ as charge carrier. Unmodulated currents (Fig. 1*A*) were measured during internal dialysis of GDPβS (2 mM), a non-hydrolysable analogue of GDP that minimizes G-protein activation (Ikeda, 1991). These records manifest many of the features of uninhibited N-type currents observed in previous studies of neurons and heterologous expression systems (Elmslie, Zhou & Jones, 1990; Ikeda, 1991; Bourinet, Soong, Stea & Snutch, 1996). Strong prepulses (45 ms) produce no appreciable effect on ionic currents observed during test depolarization (Fig. 1*A*, compare left (without prepulse) and right (with prepulse) traces). They also have no discernible effect on the voltage dependence of activation, represented as plots of normalized conductance (G/G_{max}) as a function of voltage (Fig. 1*B*). Such '*G–V*' curves were derived from peak tail currents following test depolarizations (see Methods). The dominance of a single Boltzmann distribution in the fit to *G–V* data (Fig. 1*B*, continuous line) agrees with the expectation of mainly a single population of (uninhibited) channels with GDPβS (Bean, 1989; Ikeda, 1991). All these observations reflect only N-type channel properties: 2 μM ω-CgTX completely blocked inward and outward currents (Fig. 1*B*, inset).

Comparison of the currents in control (Fig. 1*A*) with those obtained during G-protein activation (Fig. 1*C*) reveals the traditional hallmarks of voltage-dependent G-protein inhibition (Hille, 1994). In these experiments, we included GTPγS (300 μM) in the internal dialysate to activate G-proteins (Scott & Dolphin, 1988; Elmslie *et al.* 1990; Ikeda, 1991). Prepulse depolarization now strikingly increases the magnitude of both test pulse and ensuing tail currents, consistent with the notion that strong depolarization transiently relieves inhibition and returns channels towards unmodulated behaviour. The leftward shift of the *G–V* curve with prepulse (Fig. 1*D*) underscores the profound facilitative effect of prepulses. Another feature of voltage-dependent inhibition seen during GTPγS dialysis is the dual-Boltzmann shape of the *G–V* curve (Fig. 1*D*), a feature which has been previously interpreted to reflect the existence of two populations of channels (G-protein inhibited and uninhibited; Bean, 1989).

Together, these results indicate that robust, voltage-dependent G-protein inhibition of recombinant N-type channels was established under our experimental conditions.

Gating currents of uninhibited N-type channels

To isolate gating currents, we used an external block solution with 0·1 mM La^{3+} (see Methods). Figure 2*A* shows the resultant current records with minimal G-protein inhibition (GDPβS in the internal dialysate). The voltage protocol is shown at the top of the figure: traces on the left correspond to test depolarizations without a prepulse; those on the right were obtained 20 ms after a strong depolarizing prepulse. The prepulse and interpulse parameters are identical to those used for ionic current.

On the basis of extensive criteria, these traces constitute non-linear charge displacement currents that can be rigorously identified as N-type gating currents. Most importantly three essential technical prerequisites are satisfied. (1) No displacement currents are observed in mock transfected HEK 293 cells (Fig. 2*B*). (2) Membrane properties are linear over the voltages used to obtain leak subtraction templates, as demonstrated by the zero sum response to opposite polarity voltage jumps (Fig. 2*C*). The insensitivity of measured displacement currents to the choice of leak subtraction pulses (*P*/8, *P*/−8, and *P*/5), delivered from voltages between −115 and −100 mV, provides further strong support for the linearity of membrane properties over the voltage range used for leak subtraction templates (data not shown). (3) Displacement currents initially isolated with 2 μM ω-CgTX (Fig. 1*B*, inset) were not affected by the addition of La^{3+}, apart from simple surface potential shifts (see Methods). Hence, the 0·1 mM La^{3+} used to isolate gating current did not appear to distort gating properties.

Beyond the technical prerequisites, the displacement currents in Fig. 2*A* satisfied all the functional criteria for gating currents arising from a voltage-gated channel (Armstrong & Bezanilla, 1974; Armstrong, 1981; Bean & Riòs, 1989). Time integrals of outward (Q_{on}, Fig. 2*D*) and

inward (Q_{off}, Fig. 2*E*) currents saturated with increasing test depolarization. Q_{on} matched Q_{off}, as the identical fit in Figs 2*D* and *E* shows (continuous curve). Superposition of *Q–V* and *G–V* relations (Fig. 2*E*) illustrates that charge movement paralleled ionic current activation over a broad range of voltages. Finally, as expected from the behaviour of ionic currents with GDPβS (Fig. 1*A*), all properties of displacement currents were unaffected by prepulse (Fig. 2*D* and *E*, compare data ± prepulse). All these findings firmly established the non-linear displacement currents as N-type channel gating currents.

N-type channel gating currents during G-protein activation

The most important new information comes with observation of N-type channel gating currents during G-protein activation. Figure 3 summarizes gating current experiments obtained with GTPγS; the voltage protocols and ionic

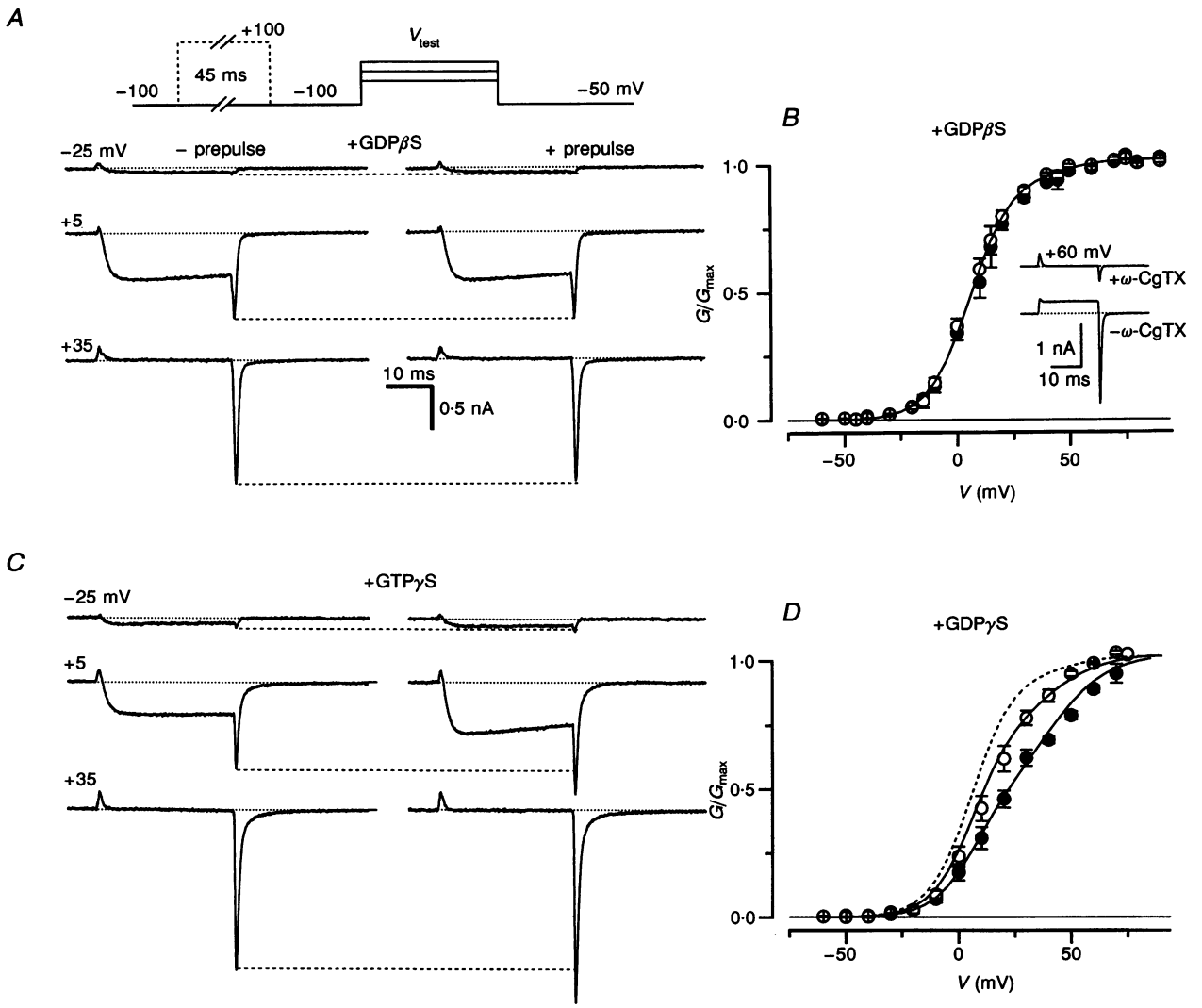

Figure 1. G-protein modulation of ionic currents from recombinant N-type channels

A, ionic currents during dialysis with GDPβS. Voltage protocol shown at top. Records show the response to test pulse depolarizations with (right traces) or without (left traces) prepulse. *B*, *G–V* curves, averaged from >10 cells (○, with prepulse; ●, without prepulse). Continuous curve is dual-Boltzmann fitted to *G–V* data with prepulse ($Z_{lo} = 2{\cdot}8$, $Z_{hi} = 2{\cdot}7$, $V_{½,lo} = 7$ mV, $V_{½,hi} = 50$ mV; $f_{lo} = 0{\cdot}97$ and $f_{hi} = 0{\cdot}06$; here and in subsequent figure legends, for explanation of abbreviations see equation in Methods). Inset, 2 μM ω-CgTX (top) blocks all ionic current (bottom). *C*, format as in *A*, now during GTPγS dialysis. Independent of the test potential, tail currents decayed with a biexponential time course, with approximately 90% of the amplitude represented by a $\tau \approx 0{\cdot}6$ ms component, and 10% by a $\tau \approx 4{\cdot}4$ ms component. *D*, *G–V* curves, averaged from > 5 cells (○, with prepulse; ●, without prepulse). Continuous lines are dual-Boltzmann fits ($Z_{lo} = 2{\cdot}9$, $Z_{hi} = 1{\cdot}9$, $V_{½,lo} = 6$ mV, $V_{½,hi} = 10{\cdot}6$ mV; f_{lo} and f_{hi} values were 0·44 and 0·58 without prepulse or 0·73 and 0·29 with prepulse, respectively). Dashed line reproduces fit in *B*. Data and fits in *B* and *D* are shifted +12 mV for surface charge (see Methods).

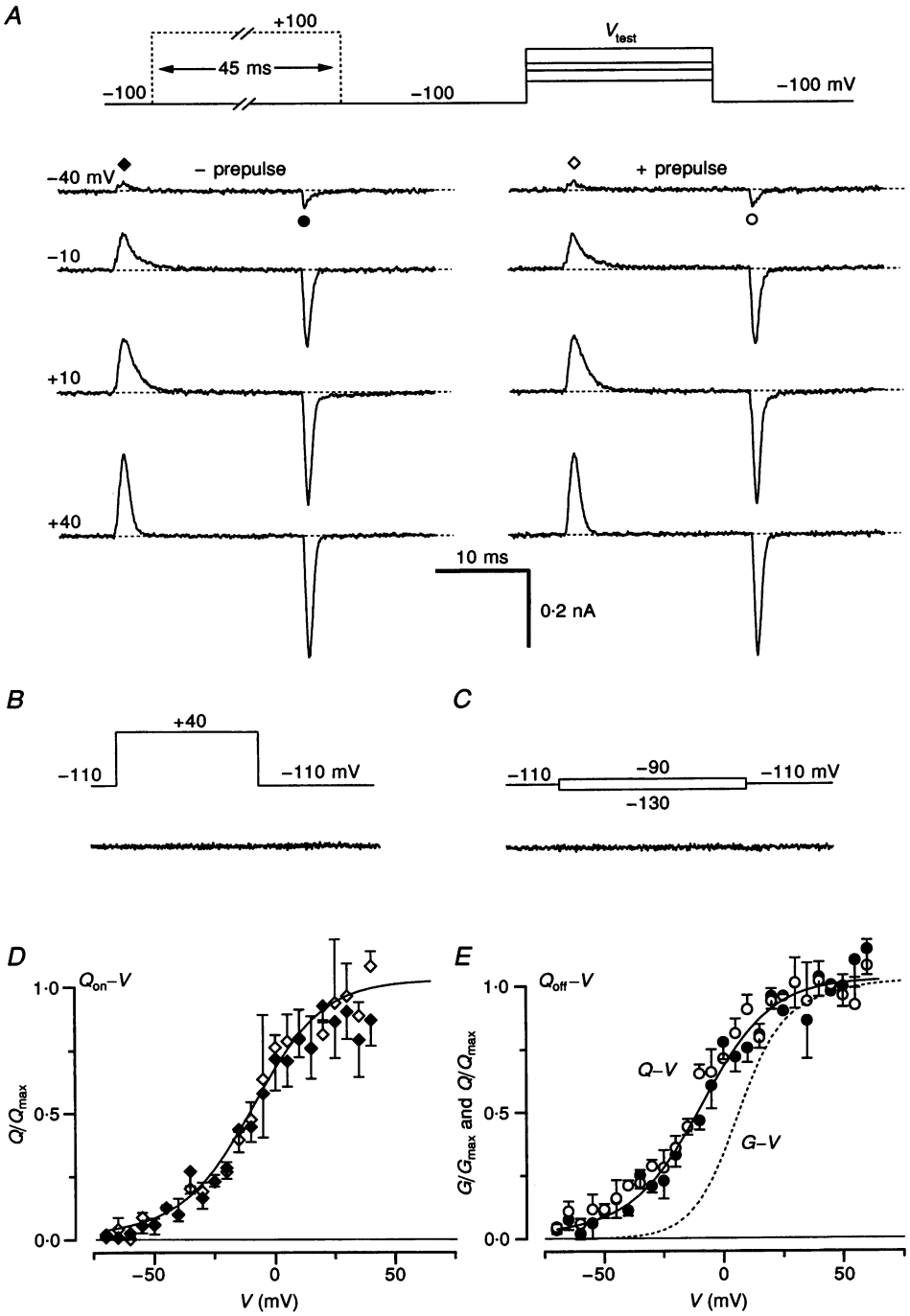

Figure 2. Gating currents from uninhibited N-type channels

A, gating current during dialysis with GDPβS. Voltage protocol shown at top. Records show response to test pulse depolarization with (right column) or without (left column) prepulse. All traces averaged from three trials. *B*, absence of gating currents in mock-transfected cell. *C*, zero sum response to opposite polarity voltage jumps, indicating linearity of membrane properties over voltage range used to obtain leak templates. Cell with 0·6 nA of peak N-type ionic current at 0 mV. *D*, Q_{on}–V relations, averaged from 3–7 cells (◆, without prepulse; ◇, with prepulse). Continuous curve shows dual-Boltzmann fit ($Z_{lo} = 1{\cdot}7$, $Z_{hi} = 2{\cdot}5$, $V_{½,lo} = -15$ mV, $V_{½,hi} = 10$ mV; $f_{lo} = 0{\cdot}85$ and $f_{hi} = 0{\cdot}17$). *E*, Q_{off}–V relations, averaged from same cells as in *D* (●, without prepulse; ○, with prepulse). Continuous curve is same fit as in *D*. Dashed curve is the fit to G–V curve with prepulse in Fig. 1*D*. Before averaging across cells, all Q–V curves (*D* and *E*) were normalized by Q_{max}, an estimate for the maximum mobile charge (see Methods). Therefore, the absolute gating charge amplitudes in *D* and *E* can be gauged from the average value of Q_{max} ($3{\cdot}22 \pm 1{\cdot}6$ fC pF^{-1} ($n = 7$)).

conditions are identical to those in Fig. 2. For each cell in this series, we first measured ionic currents (as in Fig. 1) to ensure that prepulse facilitation was present and stable over time. In eight cells, we were also able to remeasure ionic currents following gating current measurements. There was no significant change in the level of G-protein modulation, as gauged by the ratio of peak test currents at 0–5 mV with prepulse divided by those without prepulse (1·69 ± 0·11 before, compared with 1·78 ± 0·09 after, gating current measurements, $P > 0{\cdot}05$, Student's paired t test). We therefore infer that the level of G-protein inhibition was quite stable throughout gating current experiments.

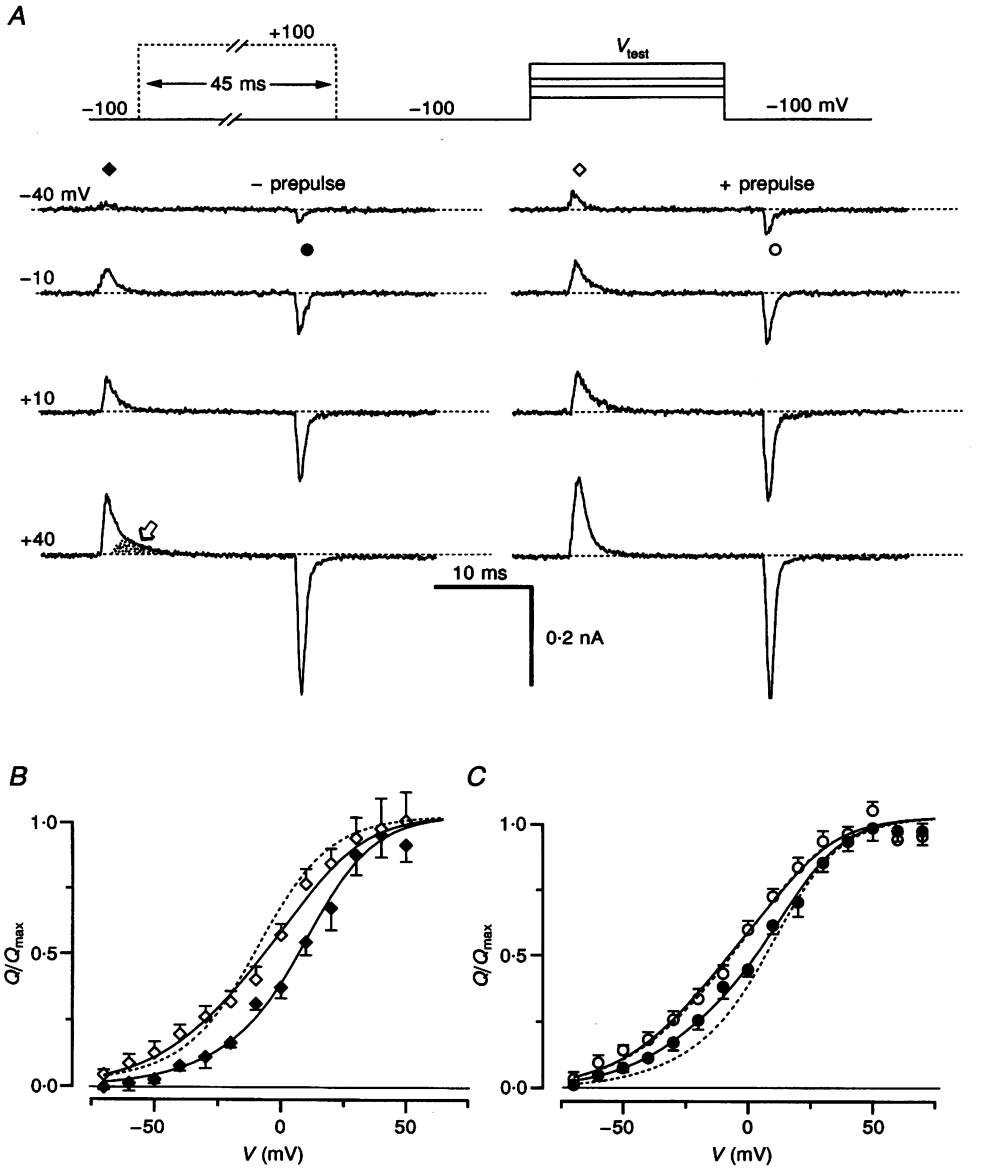

Figure 3. Gating currents during G-protein inhibition of N-type channels

A, gating current during dialysis with GTPγS. Identical format to Fig. 2*A*. *B*, Q_{on}–V relations, averaged from 6 cells (◆, Q_{on} without a prepulse); ◇, Q_{on} with a prepulse)). Continuous curves are dual-Boltzmann fits ($Z_{lo} = 1{\cdot}4$, $Z_{hi} = 2{\cdot}0$, $V_{½,lo} = -20$ mV, $V_{½,hi} = 12$ mV; f_{lo} and f_{hi} values were 0·21 and 0·81 without a prepulse and 0·64 and 0·4 with a prepulse, respectively). Dashed line reproduces Q–V fit for uninhibited channels from Fig. 2*D*. *C*, Q_{off}–V relations, averaged from same cells (●, Q_{off} without a prepulse; ○, Q_{off} with a prepulse). Continuous curves are dual-Boltzmann fits to the Q_{off}–V data ($Z_{lo} = 1{\cdot}4$, $Z_{hi} = 2{\cdot}2$, $V_{½,lo} = -19$ mV, $V_{½,hi} = 16$ mV; f_{lo} and f_{hi} values were 0·46 and 0·57 without a prepulse and 0·7 and 0·3 with a prepulse). Dashed lines reproduce fits to Q_{on}–V relations in *B*. Absolute gating charge in *B* and *C* can be gauged from the average Q_{max} value as described in Fig. 2 legend. Here, the average Q_{max} was 4·04 ± 0·7 fC pF^{-1} ($n = 6$), which is not statistically different ($P > 0{\cdot}4$, Student's two-sided t test) from the analogous Q_{max} obtained with GDPβS (see Fig. 2 legend).

The gating currents elicited during G-protein activation (Fig. 3*A*) exhibit striking modulatory effects. Without a prepulse, gating charge movement appears inhibited at modest test depolarizations, an effect that is clearly illustrated by the reduction of gating currents at −40 mV with GTPγS (Fig. 3*A*, left), compared with those observed under unmodulated conditions (GDPβS, Fig. 2*A*). Even more clear-cut is the increased amplitude of gating currents following prepulse (Fig. 3*A*, right with prepulse). The facilitation is prominent at test potentials $\leqslant 10$ mV. At more depolarized potentials, the overall augmentation of gating current is less, as if all the gating charge of inhibited channels can eventually be moved with sufficient test depolarization. The Q–V curves confirm this proposal: the prepulse does not appreciably change the maximum amplitude of either Q_{on}–V (Fig. 3*B*) or Q_{off}–V (Fig. 3*C*) relations. Instead, the prepulse acts to produce a hyperpolarizing shift in Q_{on}–V (Fig. 3*B*) and Q_{off}–V (Fig. 3*C*) relations. In fact, the Q–V relation obtained after prepulse (Fig. 3*B*, ◇) is shifted so much that it nearly approximates the Q–V curve for unmodulated channels, represented here by the fit to data with GDPβS (dashed line). The close approximation of Q–V curves, together with the overall similarity of gating currents following prepulse (Fig. 3*A*, right) to those observed with GDPβS (Fig. 2*A*), emphasizes the large extent to which strong prepulses returned channels towards their unmodulated behaviour.

G-protein effects were not limited to changes in gating current amplitude. Comparison of Q_{on}–V and Q_{off}–V relations obtained with GTPγS (Fig. 3*C*, dashed lines are Q_{on}–V fits) suggests the existence of kinetic effects, as follows. Q_{on} is clearly smaller than Q_{off} in the absence of prepulse depolarization. This discrepancy is unlikely to arise from a technical artifact, because of the complete agreement of Q_{on} and Q_{off} with prepulse (Fig. 3*C*, GTPγS), as well as with GDPβS (Fig. 2*D* and *E*, with or without a prepulse). Rather, the difference between Q_{on} and Q_{off} in the absence of a prepulse argues that part of the gating charge of inhibited channels moves very slowly during activation, consequent to a marked reduction of certain rate constants leading to the open state. Such an ultra-slow component of charge movement could easily be lost in the baseline subtraction procedure used to evaluate Q_{on} (see Methods). However, all the gating charge moved during the test depolarization should be detectable during repolarization (Q_{off}) because rate constants leading to deactivation should, if anything, be accelerated in G-protein-inhibited channels. Accordingly, Q_{off} would exceed Q_{on}. A prediction made by this scenario is that the increase in the amount and the rate of charge movement at higher test depolarizations should reveal the slow gating current component of inhibited channels. In fact, at +40 mV the outward gating current without prepulse has a prominent slow component (Fig. 3*A*, arrow and stippling in +40 mV trace), which is smaller in the comparable trace with prepulse (Fig. 3*A*, right), and absent in gating currents with GDPβS (Fig. 2*A*).

DISCUSSION

We have resolved gating currents arising solely from voltage-sensor movements of N-type calcium channels, taking advantage of recombinant expression of calcium channel α_{1B}-, β_{1b}- and α_2-subunits in HEK 293 cells. Although much research has clearly established that G-proteins inhibit ionic currents in a manner that can be transiently reversed by strong depolarization (Elmslie *et al.* 1990; Ikeda, 1991; Hille, 1994), only here have we demonstrated modulatory effects on gating charge movements. G-proteins inhibited charge movement during small test depolarizations, and shifted Q–V curves to more positive voltages. Prepulse depolarization largely reversed the effects, returning Q–V curves towards their unmodulated counterparts.

Although modulation of voltage-gated channels is ubiquitous, N-type calcium channels may provide the first clear example of acute, physiological regulation involving dramatic alteration of gating-charge behaviour. For example, in the case of L-type calcium channels, β-adrenergic modulation produces no (Bean, 1990; Hadley & Lederer, 1991) or subtle (Josephson & Sperelakis, 1991) effects on gating current, despite marked enhancement of ionic currents. Moreover, robust Ca^{2+} inactivation of current is also devoid of appreciable changes in gating current (Hadley & Lederer, 1991; Shirokov, Levis, Shirokov & Riòs, 1993). Hence, these other modulatory systems act mainly to modify weakly voltage-dependent transitions near the open state, those corresponding to coupling of voltage-sensor activation and channel opening (G–Q coupling). In contrast to all the examples of exclusive effects on G–Q coupling, the prominent regulation of N-type channel gating current implicates significant action on the voltage sensors, an effect that is so far unique.

To consider the mechanistic implications of our data, we first summarize the current understanding of G-protein modulation of N-type channels, shown in coarse outline by Fig. 4*A* (Elmslie *et al.* 1990; Boland & Bean, 1993; Patil *et al.* 1996). Uninhibited channels gate according the upper row of closed (C) and open (O) states, collectively referred to as a 'willing' mode of gating (Bean, 1989). Here, moderate depolarization permits ready opening of the channel. Binding of G-protein βγ-subunits (vertical transitions) translocates the channel to the bottom row of states, which comprise a 'reluctant' mode. In this mode, transitions to the open state ($O_{1'}$) are virtually prohibited at modest depolarization. Thus, activation of G-proteins leads to inhibition of ionic current by increasing the fraction of channels in the reluctant mode (G-protein bound). In contrast, prepulse depolarization drives channels rightward (from states C_R and $C_{R'}$, the deepest resting state of willing and reluctant modes, respectively) towards states that are presumed to have decreased G-protein affinity (schematized by relative lengths of vertical transition arrows). Prepulses thereby induce transient G-protein release and temporary enrichment of the willing fraction of channels. Accordingly, current is

facilitated in a subsequent test pulse. Outside these broad points of consensus, major questions remain as to the voltage dependence of transitions in the normal activation pathway, as well as to the steps at which G-proteins act to retard activation in the reluctant mode.

Comparison of G–V and Q–V relations during G-protein activation lends crucial insight into these open questions. Figure 4*B* and *C* shows the G–V data corresponding to the Q–V relations obtained with GTPγS. The Q–V data were already presented in Fig. 3, so only the fit to Q_{off}–V data is reproduced in Fig. 4 as dashed curves. The explicit matchup between G–V and Q–V curves underscores a striking, fundamental result: although G-proteins clearly alter Q–V curves (Fig. 3), G-proteins exert their greatest effect on the interrelation between G–V and Q–V curves, as demonstrated by the remarkable contrast between Fig. 4*B* (with prepulse) and *C* (without prepulse). The nature of these large modulatory effects provides the basis for deducing the overall structure of voltage dependence in the normal activation pathway. In addition, they enable identification of specific groups of transitions at which G-proteins retard activation of reluctant channels. We argue as follows.

After prepulse (Fig. 4*B*), Q–V and G–V relations mainly represent the behaviour of channels without G-proteins (in the willing mode), as the close similarity to analogous curves with GDPβS confirms (Fig. 2*E*). The interrelation between these curves (Fig. 4*B*) points to three functional groups of transitions in the willing mode (a, b, and c in Fig. 4*A*). The leftmost transitions comprise group a. Because of the separation between group a and the open state (O_1), voltage-dependent transitions in this group can account for the initial component of charge movement that occurs before ionic activation. About half the total amount of mobile charge ($\sim Q_T/2$) is associated with group a. As voltage increases beyond 0 mV, the final half of the rise of Q–V and G–V curves almost superimpose. This strongly suggests that the remaining half of charge movement is associated with a near rate-limiting set of activation step(s) to the right of

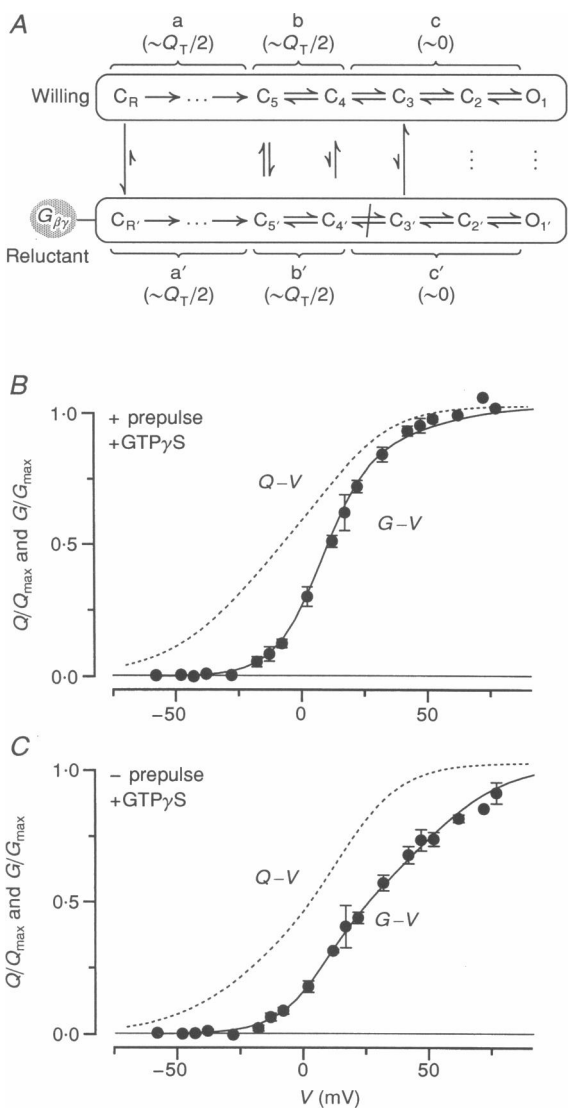

Figure 4. Mechanistic implications of G-protein effects on G–V and Q–V relations

A, proposed effects of G-proteins on charge movement and channel activation. Abbreviations are: Q_T, total amount of mobile charge; C_R, a deep resting state; $G_{\beta\gamma}$, G-protein $\beta\gamma$ subunits; broken arrow is a restriction in transmission due to G-protein; for further explanation see text. *B*, comparison of G–V and Q_{off}–V relations obtained with 300 μM intracellular GTPγS, with prepulse. Dashed line reproduces fit to Q_{off}–V (with a prepulse) in Fig. 3*C*. G–V data averaged from 3–7 cells, using 20 ms test depolarizations. Continuous line is dual-Boltzmann fit to G–V data ($Z_{lo} = 2{\cdot}8$, $Z_{hi} = 1{\cdot}5$, $V_{½,lo} = 8$ mV, $V_{½,hi} = 13$ mV; $f_{lo} = 0{\cdot}86$, $f_{hi} = 0{\cdot}17$). *C*, same format as *B*, now with no prepulse. Dashed line reproduces fit to Q_{off}–V (without prepulse) in Fig. 3*C*. G–V data averaged from same cells as in *B*, with dual-Boltzmann fit as continuous line ($Z_{lo} = 2{\cdot}8$, $Z_{hi} = 1{\cdot}5$, $V_{½,lo} = 8$ mV, $V_{½,hi} = 13$ mV; $f_{lo} = 0{\cdot}4$, $f_{hi} = 0{\cdot}62$). G–V data and curves are shifted to the right by +12 mV to account for surface charge (see Methods).

group a. This set of steps comprises group b. Finally, the generally weak voltage dependence of transitions near the open state in both calcium channels (Hadley & Lederer, 1995), and other voltage-gated channels (Zagotta, Hoshi & Aldrich, 1989; Vandenberg & Bezanilla, 1991), makes it likely that transitions near the open state (group c) involve little charge movement. The $C_3 = C_2 = O_1$ structure of group c is supported by our recent single-channel analysis (Patil *et al.* 1996).

Without prepulse (Fig. 4*C*), the overall shape of the *Q–V* relation is similar to that following prepulse (Fig. 4*B*), suggesting that reluctant transitions still form an analogous set of functional groups (a′, b′, c′ in Fig. 4*A*). However, specific features of *G–V* and *Q–V* curves reveal that G-proteins produce two major differences in the activation pathway. First, shifts at the foot of *Q–V* curves (with or without prepulse) where channels hardly open suggest that G-proteins slow rightward transitions in group a′ (compare Fig. 4*B* and *C*; also see Fig. 3*B* and *C*). This corresponds to direct effects of G-proteins on voltage sensor movement. A second action of G-proteins is apparent at strongly positive voltages. Here, the interrelation of *G–V* and *Q–V* curves is profoundly affected by the presence of a prepulse (compare Fig. 4*B* and *C*). In the absence of a prepulse (Fig. 4*C*), the *G–V* curve rises steeply with voltage despite the virtual saturation of the *Q–V* curve, and there is now a marked separation between *G–V* and *Q–V* curves along the voltage axis. These features point to a rate limitation to opening in the weakly voltage-dependent transitions of group c′, rather than in group b′. Hence, the second action of G-proteins is to decouple charge movement from channel opening. For simplicity, we represent the effect as a restriction in only the $C_{4'} \rightarrow C_{3'}$ transition (Fig. 4*A*, broken arrow). Interestingly, at moderate depolarizations, ~0 mV, the transition from $C_{4'} \rightarrow C_{3'}$ may be fully blocked thereby precluding access to the reluctant open state (O′) and requiring reluctant channels to release G-proteins in order to open (reaching O). Because of presumably slow kinetics of interchange between states $C_{4'}$ and C_4, openings to O would only be observed after long latencies lasting hundreds of milliseconds. Hence, the restriction to transition from $C_{4'} \rightarrow C_{3'}$ provides an explicit biophysical mechanism for our recent single-channel observations of exactly such 'preferential exchange' behaviour (Patil *et al.* 1996).

Although the precise number and connectivity of states within each group is not yet specified, we are encouraged that even this initial characterization of gating currents has provided insight into the major loci of G-protein blockade and the structure of voltage dependence of N-type channel gating. It will be interesting to see if these core properties of N-type channel activation turn out to be general design features shared widely by other members of the family of voltage-gated calcium channels.

Armstrong, C. M. (1981). Sodium channels and gating currents. *Physiological Reviews* **61**, 644–683.

Armstrong, C. M. & Bezanilla, F. (1974). Charge movement associated with the opening and closing of the activation gates of Na channels. *Journal of General Physiology* **63**, 533–552.

Bean, B. P. (1989). Neurotransmitter inhibition of neuronal calcium currents by changes in c channel voltage dependence. *Nature* **340**, 153–156.

Bean, B. P. (1990). β-Adrenergic regulation of cardiac calcium channels: ionic and gating current. *Biophysical Journal* **57**, 23a.

Bean, B. P. & Rios, E. (1989). Nonlinear charge movement in mammalian cardiac ventricular cells: components from Na and Ca channel gating. *Journal of General Physiology* **94**, 65–93.

Berjukow, S., Doring, F., Froschmayr, M., Grabner, M., Glossmann, H. & Hering, S. (1996). Endogenous calcium channels in human embryonic kidney (HEK293) cells. *British Journal of Pharmacology* **118**, 748–754.

Boland, L. M. & Bean, B. (1993). Modulation of N-type calcium channels in bullfrog sympathetic neurons by luteinizing hormone-releasing hormone: kinetics and voltage dependence. *Journal of Neuroscience* **13**, 516–533.

Bourinet, E., Soong, A., Stea, A. & Snutch, T. P. (1996). Determinants of the G-protein dependent opioid modulation of neuronal calcium channels. *Proceedings of the National Academy of Sciences of the USA* **93**, 1486–1491.

Brust, P., Simerson, S., McCue, A. F., Deal, C., Schoonmaker, S., Williams, M. E., Velicelebi, G., Johnson, E. C., Harpold, M. M. & Ellis, S. B. (1993). Human neuronal voltage-dependent calcium channels: studies on subunit structure and role in channel assembly. *Neuropharmacology* **32**, 1089–1103.

Chen, T. Y., Peng, Y. W., Dhallan, R. S., Ahamed, B., Reed, R. R. & Yau, K.-W. (1993). A subunit of the cyclic nucleotide-gated cation channel in retinal rods. *Nature* **362**, 764–767.

Dhallan, R. S., Yau, K.-W., Schrader, K. A. & Reed, R. (1990). Primary structure and functional expression of a cyclic nucleotide-activated channel from olfactory neurons. *Nature* **347**, 184–187.

Dubel, S. J., Starr, T. V., Hell, J., Ahlijanian, M. K., Enyeart, J. J., Catterall, W. A. & Snutch, T. P. (1992). Molecular cloning of the alpha subunit of an omega-conotoxin-sensitive calcium channel. *Proceedings of the National Academy of Sciences of the USA* **89**, 5058–5062.

Elmslie, K. S., Zhou, W. & Jones, S. W. (1990). LHRH and GTP-γ-S modify calcium current activation in bullfrog sympathetic neurons. *Neuron* **5**, 75–80.

Gorman, C. M., Gies, D. R. & McCray, G. (1990). Transient production of proteins using an adenovirus transformed cell line. *DNA and Protein Engineering Techniques* **2**, 3–10.

Hadley, R. W. & Lederer, W. J. (1991). Ca^{2+} and voltage inactivate Ca^{2+} channels in guinea-pig ventricular myocytes through independent mechanisms. *Journal of Physiology* **444**, 257–268.

Hadley, R. W. & Lederer, W. J. (1995). Nifedipine inhibits movement of cardiac calcium channels through late, but not early, gating transitions. *American Journal of Physiology* **269**, H1784–1790.

Herlitze, S., Garcia, D. E., Mackie, K., Hille, B., Scheuer, T. & Catterall, W. A. (1996). Modulation of Ca^{2+} channels by G-protein βγ subunits. *Nature* **380**, 258–262.

Hille, B. (1994). Modulation of ion-channel function by G-protein-coupled receptors. *Trends in Neurosciences* **17**, 531–536.

IKEDA, S. (1991). Double-pulse calcium channel facilitation in adult rat sympathetic neurons. *Journal of Physiology* **439**, 181–214.

IKEDA, S. (1996). Voltage-dependent modulation of N-type calcium channels by G-protein $\beta\gamma$ subunits. *Nature* **380**, 255–258.

JOSEPHSON, I. & SPERELAKIS, N. (1991). Phosphorylation shifts the time-dependence of cardiac Ca^{2+} channel gating currents. *Biophysical Journal* **60**, 491–497.

LIPSCOMBE, D., KONGSAMUT, S. & TSIEN, R. W. (1989). α-adrenergic inhibition of sympathetic neurotransmitter release mediated by modulation of N-type calcium channel gating. *Nature* **340**, 639–642.

MARSHALL, J., MOLLOY, R., MOSS, G. W. J., HOWE, J. R. & HUGHES, T. E. (1995). The jellyfish green fluorescent protein: A new tool for studying ion channel expression and function. *Neuron* **14**, 211–215.

NEHER, E. (1992). Correction for liquid junction potentials in patch clamp experiments. *Methods in Enzymology* **207**, 123–130.

PATIL, P., DE LEON, M., REED, R., DUBEL, S., SNUTCH, T. P. & YUE, D. T. (1996). Elementary events underlying voltage-dependent G-protein inhibition of N-type calcium channels. *Biophysical Journal* **71**, 2509–2521.

PRAGNELL, M., SAKAMOTO, J., JAY, S. D. & CAMPBELL, K. P. (1991). Cloning and tissue-specific expression of the brain calcium channel beta-subunit. *FEBS Letters* **291**, 253–258.

SCOTT, R. H. & DOLPHIN, A. C. (1988). The agonist effect of Bay K 8644 on neuronal calcium channel currents is promoted by G-protein activation. *Neuroscience Letters* **89**, 170–175.

SHIROKOV, R., LEVIS, R., SHIROKOVA, N. & RIOS, E. (1993). Ca^{2+}-dependent inactivation of cardiac L-type Ca^{2+} channels does not affect their voltage sensor. *Journal of General Physiology* **102**, 1005–1030.

SUN, D. D., CHANG, F. C., CHIEN, A., XHAO, X.-L., SHIROKOV, R., RIOS, E. & HOSEY, M. (1994). Expression of functional cardiac L-type Ca^{2+} channels in transiently transfected HEK (293) cells. *Biophysical Journal* **66**, A320.

TOMLINSON, W. J., STEA, A., BOURINET, E., CHARNET, P., NARGEOT, J. & SNUTCH, T. P. (1993). Functional properties of a neuronal class C L-type calcium channel. *Neuropharmacology* **32**, 1117–1126.

VANDENBERG, C. A. & BEZANILLA, F. (1991). A sodium channel gating model based on single channel, macroscopic ionic and gating currents in the squid giant axon. *Biophysical Journal* **60**, 1511–1533.

VERDOORN, T. A., DRAGUHN, A., YMER, S., SEEBURG, P. H. & SAKMANN, B. (1990). Functional properties of recombinant rat $GABA_A$ receptors depend upon subunit composition. *Neuron* **4**, 919–928.

ZAGOTTA, W. N., HOSHI, T. & ALDRICH, R. W. (1989). Gating of single *Shaker* potassium channels in Drosphila muscle and in *Xenopus* oocytes injected with *Shaker* mRNA. *Proceedings of the National Academy of Sciences of the USA* **86**, 7243–7247.

Acknowledgements

We thank K. P. Campbell for the β_{1b} clone, J. G. Mulle for technical assitance, and D. L. Brody and D. M. Cai for discussion and comments. This work was supported by a National Science Foundation Presidential Faculty Fellowship (D.T.Y.), the MRC of Canada and the Howard Hughes Medical Institute (T.P.S.), and the NIH Medical Scientist Training Program Awards (L.P.J. and P.G.P.).

Author's email address

D. T. Yue: dyue@bme.jhu.edu

Received 9 August 1996; accepted 30 October 1996.